Electronic Supplementary Information

Self-Assembled Polyoxovanadate-Intercalated Layered Double Hydroxide Nanosheets Hybridized with Graphene Oxide for Extrinsic Supercapacitors

Navnath S. Padalkar,[a] Deepak P. Dubal[b] and Jong Pil Park[a]*

[a]Basic Research Laboratory, Department of Food Science and Technology, and GreenTech-based Food Safety Research Group, BK21 Four, Chung-Ang University, Anseong 17546, Republic of Korea

[b]Centre for Materials Science School of Chemistry & Physics Queensland University of Technology 2 George Street, Brisbane, QLD 4000, Australia

*E-mail: jppark@cau.ac.kr

Experimental section

Chemicals

Formamide (CH_3NO), nitric acid (HNO_3), hydrochloric acid (HCl), nickel nitrate hexahydrates ($Ni(NO_3)_2.6H_2O$), chromium nitrate nonahydrate ($Cr(NO_3)_3.9H_2O$), sodium nitrate ($NaNO_3$), sodium hydroxide (NaOH), sodium orthovanadate (Na_3VO_4), and graphite flakes were purchased from Sigma Aldrich. All chemicals were used as received, and all aqueous solutions were prepared using decarbonated water.

Synthesis of NiCr-layered double hydroxide (NC-LDH)

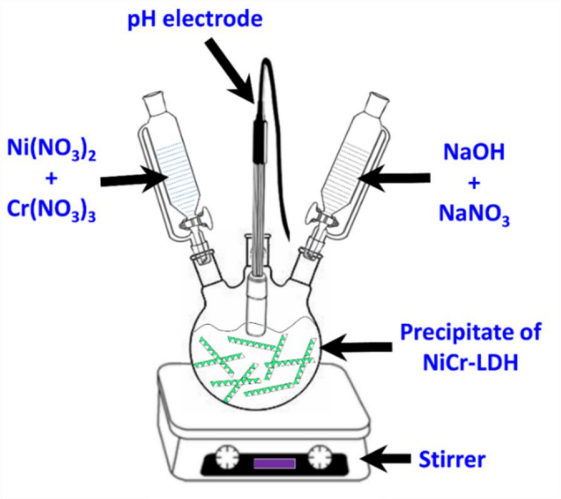

Scheme 1: Schematic diagram of co-precipitation method for the synthesis of NC–LDH.

The pristine NC-LDH was synthesized in the nitrate form using a conventional co-precipitation method (as shown in Scheme S1) at room temperature according to Rochelle protocol.[1] The aqueous cationic solution A was prepared by (0.050 M) nickel nitrate and (0.025

M) chromium nitrate solutions, and the aqueous anionic solution B was prepared by mixing (1 M) sodium hydroxide and (1 M) sodium nitrate aqueous solutions. Subsequently, solutions A and B were mixed slowly (1 ml/min) into a three-necked flask with vigorous staring at room temperature. The pH of the resultant slurry was adjusted at 8.0 +/– 0.1 by the precise addition of solution B. Then the mixed solution was placed for aging at 65^{o} C for 3 days. This synthesis process was carried out under a CO_2-free N_2 atmosphere with decarbonated water at room temperature to avoid CO_2 contamination in the LDH. After the aging process, the product was centrifuged at 7000 rpm and washed thrice with decarbonated water. Finally, the resultant product was dried in a vacuum oven at 40^{o} C for 36 h to ensure the solid form of the NC-LDH sample.

Synthesis of lattice-engineered 0D-2D-2D NCVG nanoarchitecture.

The aqueous suspension of exfoliated graphene oxide (GO) was prepared by modified Hummer's method.[2] The colloidal suspension of NC-LDH monolayers was achieved by the dispersion of pristine powder in formamide (1mg mL^{-1}) under N_2 flow. The exfoliation and the type of electrostatic charge of the NC-LDH and GO were confirmed by the Tyndall effect and zeta potential measurement (Fig. S1). The aqueous solution of POV anion was prepared by pH-controlled hydrolysis of 0.2 M Na_3VO_4 at room temperature and adjusting the pH 5.5 with 0.2 M HNO_3. The self-assembled NCVG nanoarchitectures were synthesized by rate-controlled simultaneous addition of the aqueous GO solution, POV anion solution and the colloidal suspension of exfoliated NC-LDH monolayers under constant stirring at room temperature, as shown in the schematic of the self-assembled 0D-2D-2D POV-NC-LDH-GO (NCVG) architecture synthesis in Scheme 1. As a result, immediate flocculation occurred after mixing these solutions, indicating the rapid formation of NCVG nanoarchitecture. Restacked NCVG nanoarchitecture

precipitates were recovered by centrifugation at 7000 rpm, washed three times with formamide and absolute ethanol, and dried in a vacuum oven at 40˚C for 30 h. Several weight percentage of POV/GO components were estimated at 2 wt% for NCVG-1, 4 wt% for NCVG-2, and 6 wt% for NCVG-3. The weight ratio of NC-LDH to POV/GO was controlled to achieve the layer-by-layer staking structure of NCVG nanoarchitecture. The nanoarchitectures obtained are labelled as NCVG-1, NCVG-2 and NCVG-3, respectively. The NCV nanoarchitecture was also prepared separately with a molar ratio of NC-LDH: POV adjusted to 1:1 and following the same procedure described. To avoid contamination of NC-LDH, NCV and NCVG nanoarchitecture from carbonate anions, all the reactions and processes in the present work were carried out with decarbonated water and under N_2 atmosphere. The detailed synthesis process of NC-LDH and NCVG nanoarchitecture is provided in Supporting Information.

Characterization

Powder X-ray diffraction (P-XRD) scans were performed with a Philips Xpert Pro diffractometer to study the crystal structure analysis of prepared nanoarchitecture. Fourier transform infrared spectroscopy (FTIR) absorption spectra were recorded on the VERTEX 80v spectrometer. The chemical bonding nature of NCVG nanoarchitecture was examined using VERTEX 80v spectrometer with a 532 nm excitation wavelength. The surface morphology of NC-LDH, NCV and NCVG nanoarchitectures were monitored with field emission scanning electron microscopy (FESEM, Hitachi SU8010). The stacking structure and chemical composition of the nanoarchitectures were probed with high-resolution transmission electron microscope/energy dispersive spectrometry (EDS)-elemental mapping analysis (HRTEM, JEOL JEM 2100F). X-ray photoelectron spectroscopy (XPS) survey and high-resolution scan were collected using a Thermo

Fisher Scientific K-alpha spectrometer. Nitrogen sorption isotherms were recorded on the Micrometrics 3Flex surface characterization analyzer. The prepared samples (NC-LDH, NCV, NCVG-1, NCVG-2, and NCVG-3) were degassed at 120˚C for 5 hr prior to the analysis.

Electrochemical measurement (three-electrode system)

The electrochemical performance of NC-LDH, NCV and NCVG nanoachitecture electrodes were measured using ZIVE SP1 electrochemical workstation in the three-electrode system that includes a working electrode (NC-LDH/NCV/NCVG), reference electrode (Hg/HgO) and counter electrode (Pt mesh). The 2M KOH was used as an aqueous electrolyte. Preparation of the working electrode procedure is as follows, 85 % active material (NC-LDH/NCV/NCVG/AC), 10% acetylene black and 5% polyvinylidene difluoride were mixed in N-methylpyrrolidone and grounded for 45 minutes to became homogeneous slurry. Further, the homogeneous slurry was coated on Ni foam using the doctor blade method and dried in the oven at 70˚ for 3 hr. The electrochemical performances were probed using cyclic voltammetry (CV), galvanostatic charge-discharge (GCD) and electrochemical impedance spectroscopy (EIS) techniques.

Calculations for surface capacitive and diffusion-controlled charge contribution:

The total charge Q_t accumulated on the electrode material

$$Q_t = Q_S + Q_d \qquad \text{(S1)}$$

where, Q_s and Q_d are the surface capacitive and diffusion-controlled charges, respectively. The total charge Q_t can be calculated as

$$Q_t = \int I\, dt = \int I \frac{dV}{v} = \frac{Area\ under\ the\ CV\ curve}{Voltage\ scn\ rate} \qquad \text{(S2)}$$

Therefore, if we plot different Q_t versus different scan rates v, Q_s and constant can be obtained through linear curve fitting and extrapolation. Then Q_d can be calculated as

$$Q_d = Const.\frac{1}{\sqrt{v}} = Q_t(v) - Q_s \qquad \text{(S3)}$$

Then, Q_t (C g^{-1}) plotted against the inverse of $\sqrt{v}$. The Q_s, which are just the y-axis intercept, were produced after extrapolating the parameters.

The specific capacity was calculated from the discharge curve using the following formulae:

$$Specific\ capacity = \frac{I \times \Delta t}{m} \quad \text{(C } g^{-1}\text{)} \qquad \text{(S4)}$$

$$Specific\ capacitance = C_{cd} = \frac{specific\ capacity}{\Delta V(V)} \qquad \textit{(F } g^{-1}\textit{)} \qquad \text{(S5)}$$

where I is the applied current density (A g^{-1}), Δt is the discharge time (s), m is the mass of the active materials (g), ΔV is the potential window (V).

$$Couloumbic\ efficiency = \frac{Charge\ released\ during\ discharging}{Charge\ \ stored\ during\ charging} = \frac{I_{discharge}\ \ t_{discharge}}{I_{charge}\ \ t_{charge}} \qquad \text{(S6)}$$

Where t_{charge} and $t_{discharge}$ represent the time duration of charging and discharging. I_{charge} and $I_{discharge}$ represent the charging and discharging current.

Fabrication of hybrid aqueous and solid-state supercapacitor devices

To prepare an aqueous asymmetric device (NCVG-2//KOH//AC), the NCVG-2 nanoachitecture was used as the positive electrode and the AC as the negative electrode. The aqueous 2M KOH was used as an electrolyte. The solid-state device (NCVG-2//PV-KOH//AC) was assembled using positive (NCVG-2) and negative (AC) electrodes with PVA-KOH gel electrolyte. The PVA-KOH gel electrolyte was prepared by following procedure: 3g of polyvinylalcohol (PVA) was dissolved in 30

mL of deionized water under heating at 70℃ with constant stirring and then allowed to cool to room temperature. Subsequently, 15 mL of aqueous 2M KOH solution was slowly added into the PVA solution with continuous stirring until the formation of a clear, viscous solution.

The optimal mass ratio of the positive and negative electrodes was obtained by the charge balance ($Q^+ = Q^-$) equation

$$\frac{m_p}{m_n} = \frac{C_n \times \Delta V_n}{C_p \times \Delta V_p} \quad \text{(S7)}$$

where, m_p or m_n, C_p or C_n and V_p or V_p are the mass, specific capacitance, and potential window of the positive and negative electrodes. The obtained mass ratio of positive to negative electrodes is 0.23.

The specific capacitance (C_{cd}, F g^{-1}), specific energy (Ed, Wh kg^{-1}), and specific power (Pd, kW kg^{-1}) of the aqueous and solid-state asymmetric supercapacitor devices were calculated using the following equations

$$Specific\ capacitance = \frac{I \times \Delta t}{m \times \Delta v} \quad \text{(S8)}$$

$$E = \frac{0.5 \times C_{cd} \times (\Delta V)^2}{3.6} \quad \text{(S9)}$$

$$P = \frac{E \times 3.6}{\Delta t} \quad \text{(S10)}$$

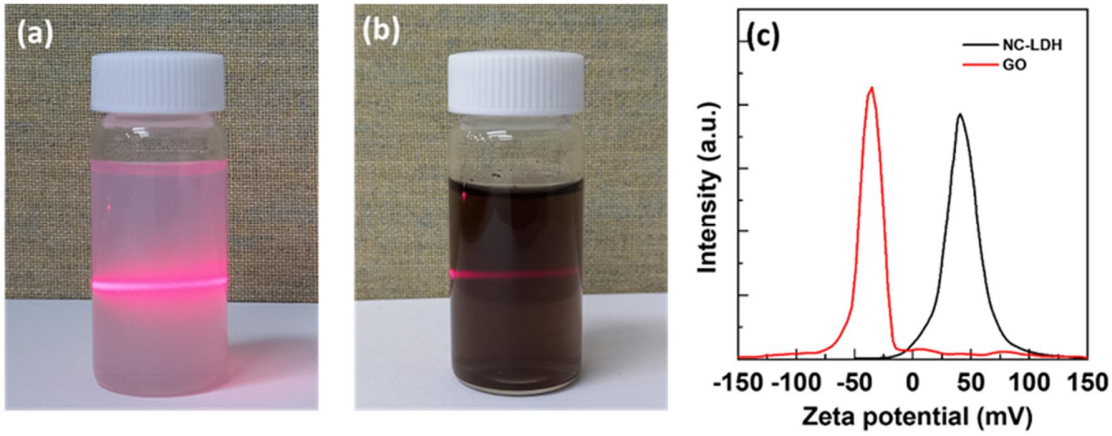

Fig. S1 Tyndall effect photograph of (a) NC-LDH, (b) GO and (c) Zeta potential curve of NC-LDH and GO nanosheets colloidal suspension.

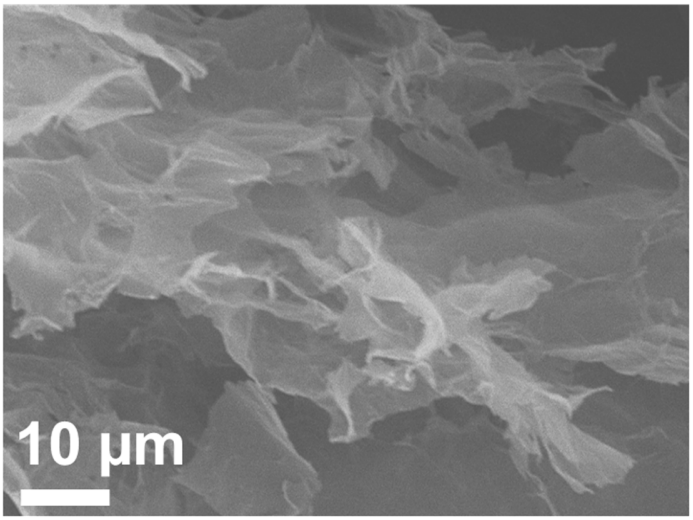

Fig. S2 FE-SEM image of GO.

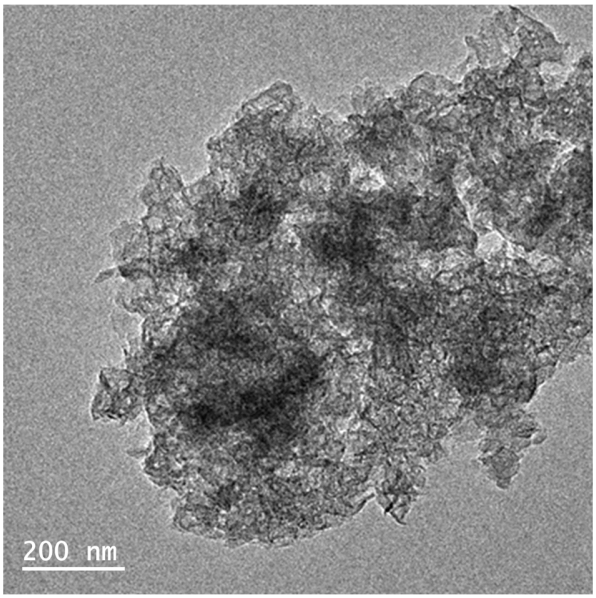

Fig. S3 TEM image of NCV nanohybrid.

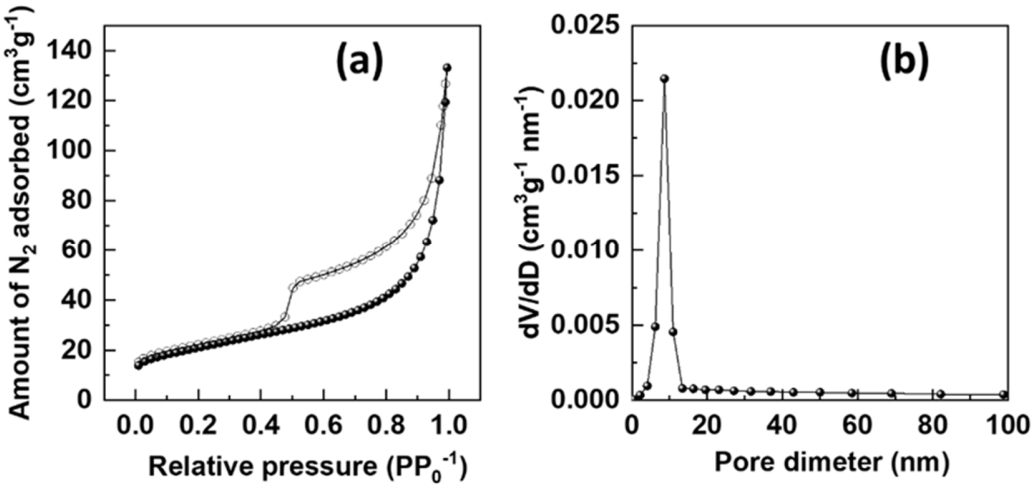

Fig. S4 (a) N_2 adsorption-desorption isotherms and (b) Pore size distribution curves calculated using the BJH equation for GO; in (a) closed and opened symbols represent the adsorption and desorption data, respectively.

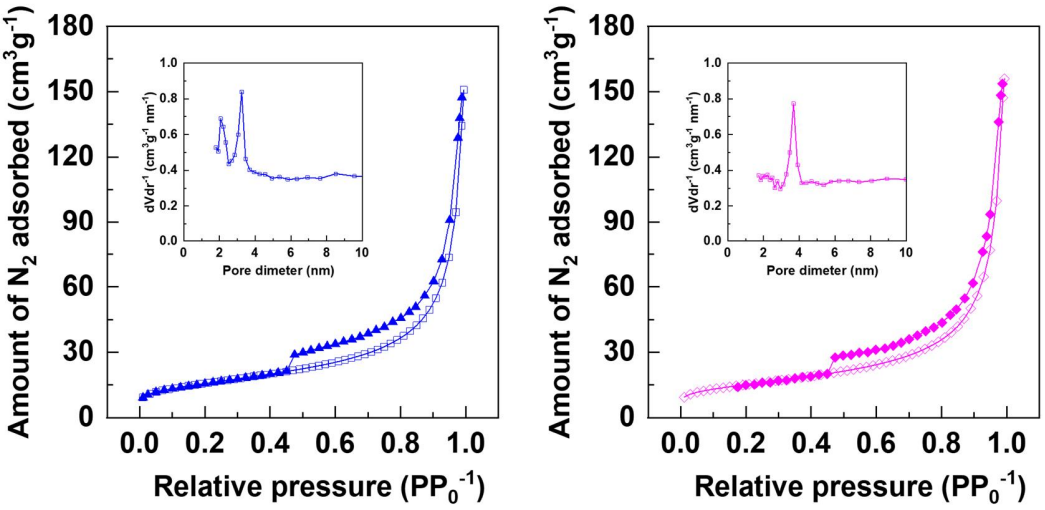

Fig. S5 N_2 adsorption-desorption isotherm and pore size distribution plot of NCVG-1 (left) and NCVG-3 (right) nanoarchiteures.

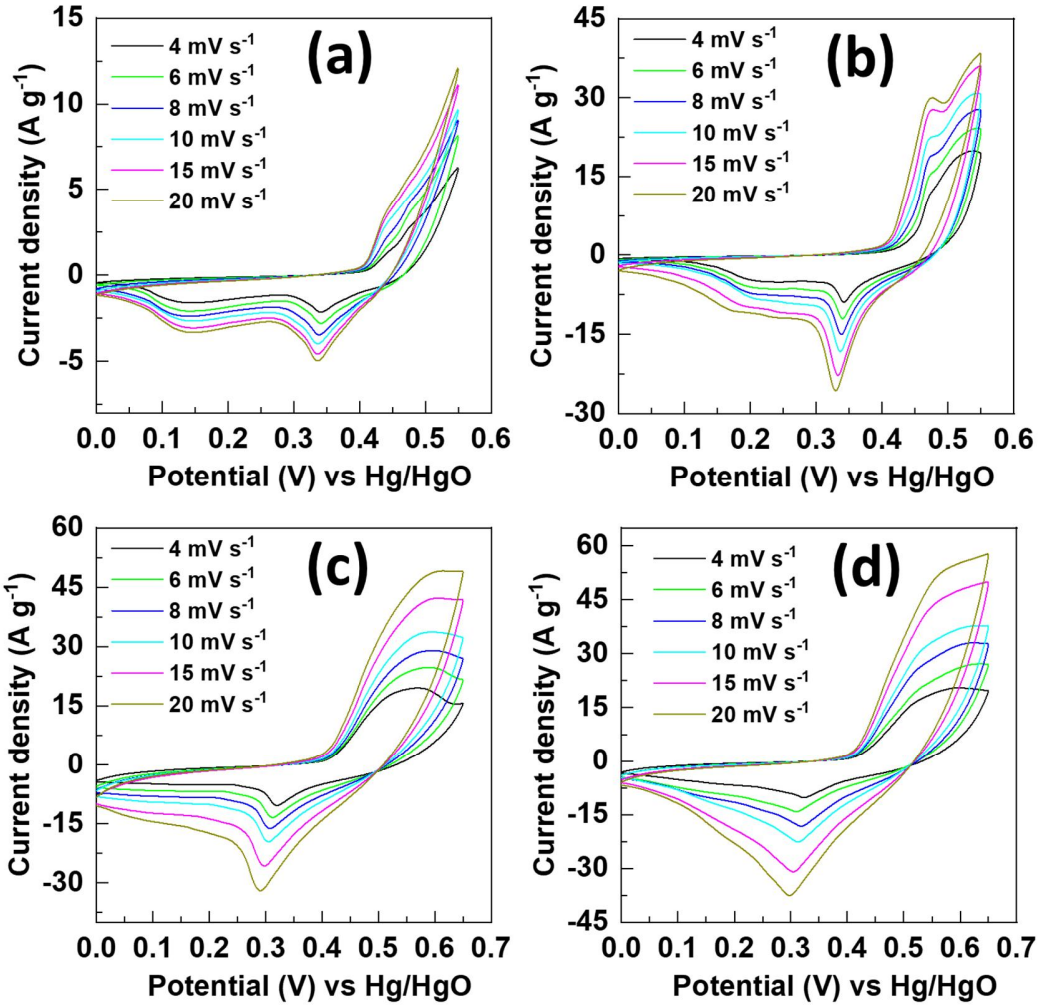

Fig. S6 The cyclic voltammetry curves of pristine (a) NC–LDH, (b) NCV, (c) NCVG-1 and (d) NCVG-3 nanoarchitecture electrodes.

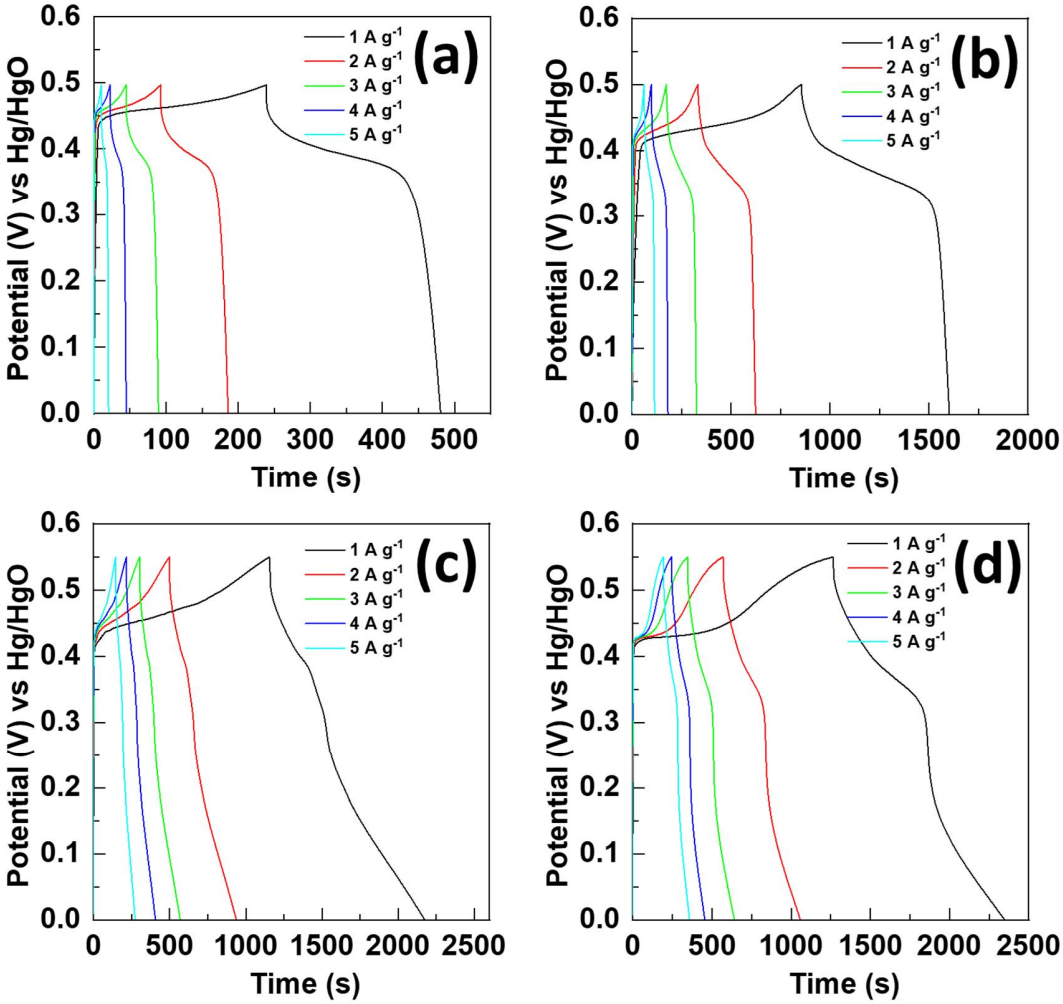

Fig. S7 The GCD curves of pristine (a) NC–LDH, (b) NCV, (c) NCVG-1 and (d) NCVG-3 nanoarchitecture electrodes.

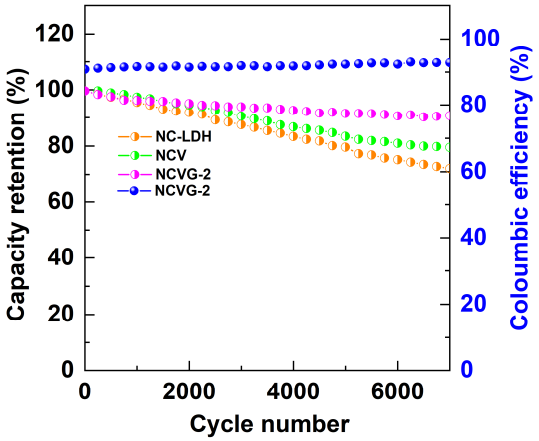

Fig. S8 Cyclic stability of pristine NC–LDH (orange), NCV (green) and NCVG-2 (pink) nanoarchitecture at 5 A g^{-1} current density. Coulombic efficiency of NCVG-2 (blue) nanoarchitecture.

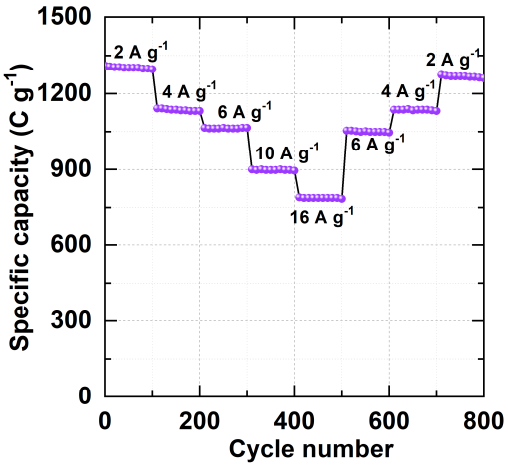

Fig. S9 Capacity of an NCVG-2 electrode cycled at various current densities: 2, 4, 6, 10, and 16 A g^{-1}.

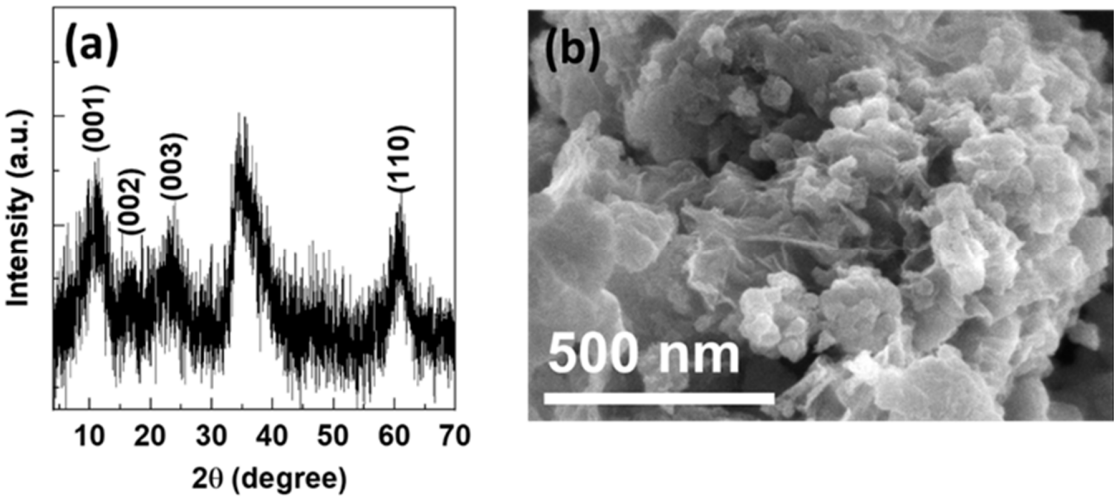

Fig. S10 (a) XRD pattern and (b) FESEM image of NCVG-2 nanoarchitecture after cycling stability (5000 GCD cycle).

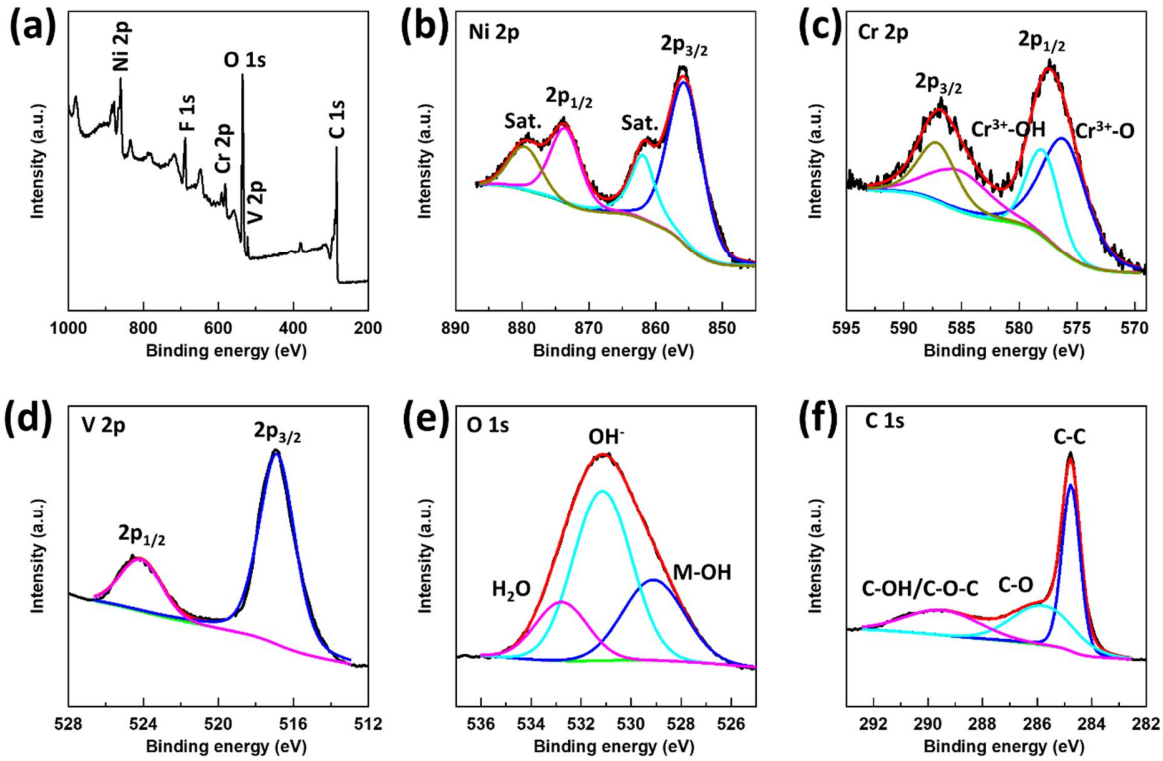

Fig. S11 (a) XPS survey spectrum of NCVG-2 nanoarchitecture. High resolution (b) Ni 2p, (c) Cr 2p, (d) V 2p, (e) O 1s, and (f) C 1s XPS spectra of NCMo-2 architecture.

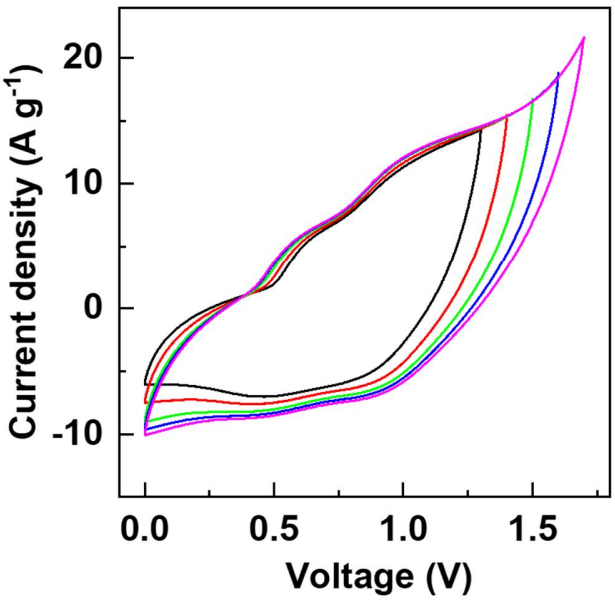

Fig. S12 The CV curves of HASSC at different voltage windows (0-1.7V).

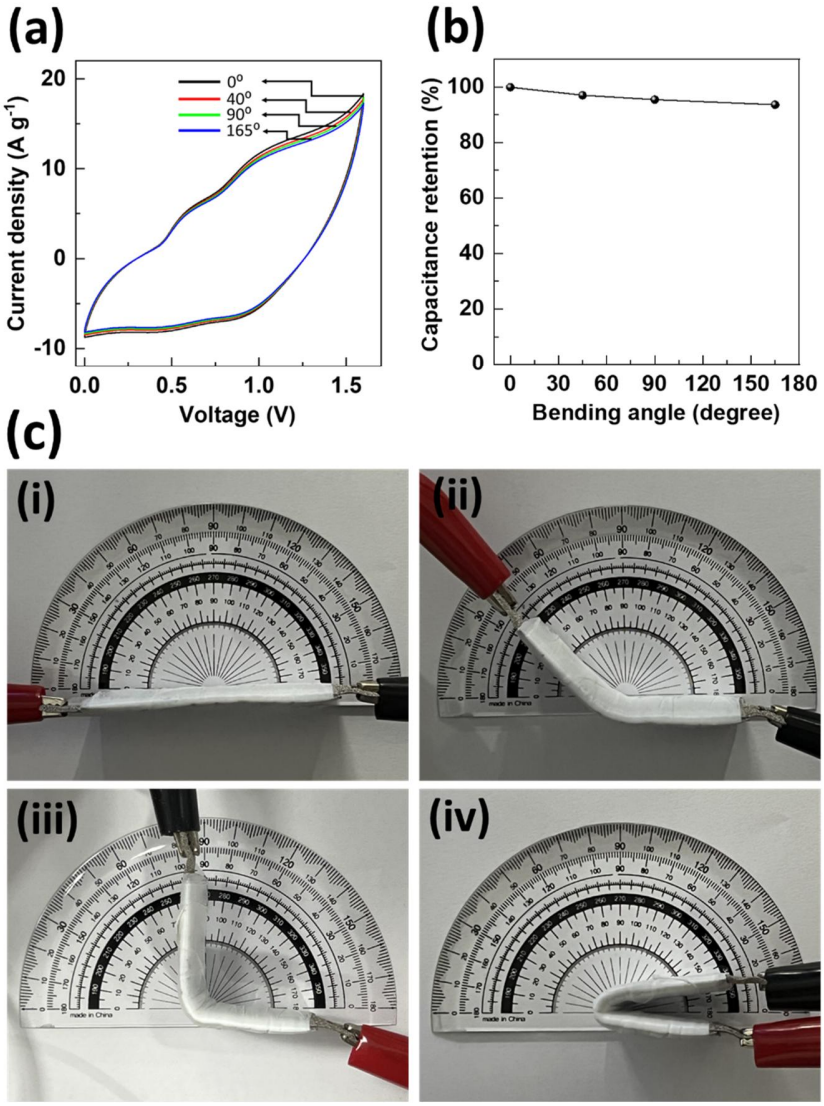

Fig. S13 (a) The CV curves of HASSC at different bending angles (0-165˚). (b) Capacitance retention of HASSC versus bending angles (0-165˚) at scan rates 100 mV s^{-1}. (c) Digital photograph of HASSC in different bending anagles of (i) 0˚, (ii) 40˚, (iii) 90˚, and (iii) 165˚.

Table S1. Comparison of LDH-based materials.

Materials	**Electrolyte/Current collector**	**Specific Capacitance /Capacity**	**Stability retention (Cyclic number)**	**Ref.**
NiCo-LDH-210	3M KOH/Nickel foam	2203.6 F g^{-1} @ 2 A g^{-1}	97.4% (2000)	[3]
CoAl LDH	6M KOH/ Nickel foam	983.1 F g^{-1} @ 1 A g^{-1}	88.84% (5000)	[4]
Ni-Co LDH/STSC-0-800	1M KOH/ Nickel foam	992.2 F g^{-1} @ 1 A g^{-1}	60% (5000)	[5]
NiCoFe-LDH	1 M KOH/Nickel foam	1990 F g^{-1} @ 1 A g^{-1}	84.8 % (5000)	[6]
CuCo-LDH	1 M KOH/Nickel foam	787 F g^{-1}@ 1 A g^{-1}	82.46% (10000)	[7]
NiCo-LDH@MOF	2M KOH/Nickel foam	723 C g^{-1} @ 1 A g^{-1}	72.5% (5000)	[8]
Co,Mn-LDH@NF	3 M KOH/ Nickel foam	2422 F g^{-1} @ 1 A g^{-1}	86.5% (3000)	[9]
NiCo-LDH/10	3 M KOH/Nickel foam	1272 C g^{-1} @ 2 A g^{-1}	103.9% (5000)	[10]
NiMn-LDH (Ov-LDH)	2M KOH/Nickel foam	1183 F g^{-1} @ 1 A g^{-1}	95 % (5000)	[11]
NiCo-LDH@PANI@CC	2M KOH/Carbon cloth	1835 F g^{-1} @ 1 A g^{-1}	78% (3000)	[12]
CoNi-LDH/$NiCo_2S_4$/RGO	2 M KOH/ Nickel foam	1846.66 F g^{-1} @ 1 A g^{-1}	93.57% (5000)	[13]
RGO/$NiCo_2S_4$/NiMo-LDH	3 M KOH/ Nickel foam	1346 F g^{-1} @ 1 A g^{-1}	-	[14]
Mo-NiS_2@NiCo-LDH	6 M KOH /Nickel foam	2604.8 F g^{-1} @ 1 A g^{-1}	-	[15]
rGO@$CoNi_2S_4$@NiCo LDH	2M KOH/Nickel foam	1310 C g^{-1} @ 1 A g^{-1}	77% (5000)	[16]
CF@NiCoZn-LDH/Co_9S_8-QD	3M KOH/ Nickel foam	2504 F g^{-1} @ 1 A g^{-1}	95.3% (8000)	[17]
CC@$NiCo_2Al_x$-LDH	1M KOH/ Carbon cloth	865 F g^{-1} @ 1 A g^{-1}	97.3% (12000)	[18]
POV-NiCr-LDH-GO	**2M KOH/ Nickel foam**	**1441 C g^{-1} (2620 F g^{-1}) @ 1 A g^{-1}**	**91% (7000)**	**Present work**

References

1 Y. Zhang, J. Cao, J. Li, Z. Yuan, D. Li, L. Wang and W. Han, *Chem. Eng. J.*, 2022, **430**, 132992.

2 M.B. Zakaria, C. Li, Q. Ji, B. Jiang, S. Tominaka, Y. Ide, J.P. Hill, K. Ariga, Y. Yamauchi Angew. Chem. Int. Edit., 2016, **55**, 8426.

3 X. Zhao, H. Li, M. Zhang, W. Pan, Z. Luo and X. Sun, *ACS Appl. Mater. Interfaces*, 2022, **14**, 34781–34792.

4 K. Li, H. Teng, X. Dai, Y. Wang, D. Wang, X. Zhang, Y. Yao, X. Liu, L. Feng, J. Rao and Y. Zhang, *CrystEngComm*, 2022, **24**, 2081–2088.

5 D. Zhang, X. Guo, X. Tong, Y. Chen, M. Duan, J. Shi, C. Jiang, L. Hu, Q. Kong and J. Zhang, *J. Alloys Compd.*, 2020, **837**, 155529.

6 J. Chen, Y. Ren, H. Zhang, J. Qi, Y. Sui and F. Wei, *Appl. Surf. Sci.*, 2021, **562**, 150116.

7 X. Chu, F. Meng, H. Yang, W. Zhang, T. Qin, Z. Wang, S. Molin, P. Jasinski and W. Zheng, *ACS Appl. Energy Mater.*, 2022, **5**, 2192–2201.

8 C. Shi, Y. Du, L. Guo, J. Yang and Y. Wang, *J. Energy Storage*, 2022, **48**, 103961.

9 D. Su, Z. Tang, J. Xie, Z. Bian, J. Zhang, D. Yang, D. Zhang, J. Wang, Y. Liu, A. Yuan and Q. Kong, *Appl. Surf. Sci.*, 2019, **469**, 487–494.

10 R. Ramachandran, Y. Lan, Z. X. Xu and F. Wang, *ACS Appl. Energy Mater.*, 2020, **3**, 6633–6643.

11 Y. Tang, H. Shen, J. Cheng, Z. Liang, C. Qu, H. Tabassum and R. Zou, *Adv. Funct. Mater.*, 2020, **30**, 1–9.

12 W. Hu, L. Chen, M. Du, Y. Song, Z. Wu and Q. Zheng, *Electrochim. Acta*, 2020, **338**, 135869.

13 Y. Guo, C. Hao, X. Wang, Y. Yang, X. Wang, J. Wu and Y. Shen, *Ceram. Int.*, 2022, **48**, 17644–17653.

14 C. Cheng, Y. Zou, F. Xu, C. Xiang, Q. Sui, J. Zhang, L. Sun and Z. Chen, *J. Energy Storage*, 2022, **52**, 105049.

15 M. Shi, M. Zhao, L. Jiao, Z. Su, M. Li and X. Song, *J. Power Sources*, 2021, **509**, 230333.

16 J. Chang, S. Zang, W. Liang, D. Wu, Z. Lian, F. Xu, K. Jiang and Z. Gao, *J. Colloid Interface Sci.*, 2021, **590**, 114–124.

17 Q. Yang, Q. Wang, Y. Long, F. Wang, L. Wu, J. Pan, J. Han, Y. Lei, W. Shi and S. Song,

Adv. Energy Mater., 2020, **10**, 1–12.

18 X. Gao, X. Liu, D. Wu, B. Qian, Z. Kou, Z. Pan, Y. Pang, L. Miao and J. Wang, *Adv. Funct. Mater.*, 2019, **29**, 1–12.